

Development of a novel method to evaluate cement sheath integrity of CCUS wells considering mechanical-chemical coupling

Chenwang Gu¹, Yongcun Feng^{1*}, Xufeng Liu², Xiaorong Li², Wei Yan³, Jingen Deng¹

1 College of Petroleum Engineering, China University of Petroleum (Beijing), China

2 College of Safety and Ocean Engineering, China University of Petroleum (Beijing), China

3. Unconventional petroleum research institute, China University of Petroleum (Beijing), China

(*Corresponding Author: yfeng@cup.edu.cn)

ABSTRACT

Wellbore integrity is crucial for the safe and effective long-term geological storage of CO₂. Over time, downhole loading and corrosion by acidic fluids can cause the mechanical strength of the cement sheath to decrease and permeability to increase, which can lead to CO₂ leakage. This paper presents a corrosion test of cement under supercritical carbon dioxide with varying times. The corrosion depth and mechanical properties of cement specimens before and after corrosion are determined through SEM tests and uniaxial and triaxial tests. A 3D numerical FEM model for cement sheath integrity is developed, which considers the coupled effects of mechanical deformation and chemical corrosion. The model is innovative and represents a new approach to analyzing cement sheath integrity. The leakage mechanism of cement sheaths under the combined effects of complex loads and chemical corrosion is analyzed by the proposed model. The results show that the corrosion depth of the cement specimens gradually increased, and the mechanical properties progressively weakened after corrosion. The radial tensile stress, micro-annulus size and equivalent plastic strain of the cement sheath increase with increasing corrosion time, indicating that the cement sheath is more susceptible to damage and debonding after corrosion. This study provides a theoretical foundation for designing new wells and assessing the suitability of existing wells for CO₂ storage.

Keywords: Cement sheath integrity, Mechanical-chemical coupling, CO₂ corrosion, CCUS, Cement failure

1. INTRODUCTION

Carbon capture, utilization, and storage (CCUS) is a vital technology for reducing carbon emissions. It involves injecting the captured CO₂ as a displacement fluid into production wells to enhance the recovery of energy such as oil, natural gas, shale gas and geothermal energy, and realize the geological storage of CO₂¹. This technology has significant benefits such as direct and rapid emission reduction and large carbon storage. It has been widely used worldwide with excellent environmental and social value^{2,3}. However, during CO₂ geological storage, CO₂ leakage remains a significant concern. In particular, the leakage problem caused by the sealing integrity failure of the cement sheath is the most prominent⁴⁻⁶. CO₂ leakage can exacerbate the greenhouse effect, lead to soil acidification, groundwater contamination, and even result in induced earthquakes and other accidents^{7,8}. Therefore, maintaining wellbore sealing integrity is crucial for successful carbon dioxide geological storage.

The cement sheath is a critical component of the wellbore barrier. The typical failure modes of the cement sheath include radial and circumferential microcracks, and interface debonding between the cement sheath and the formation or casing⁹⁻¹¹. These failure modes can result in severe consequences such as CO₂ leakage and storage failure. During well construction and service, the stresses and strains in the cement sheath are constantly changing due to complex loading conditions, such as casing pressure, in-situ stress, and temperature changes, which can easily lead to damage and failure of the cement sheath^{12,13}. During the geological storage of carbon dioxide, the cement sheath is also affected by the corrosion of acidic solution¹⁴. CO₂ dissolves in water to

form carbonic acid, which decreases the pH of the solution. Calcium oxide and calcium hydroxide in the cement sheath react with carbonic acid, which changes the distribution and morphology of the cement pore structure, decreasing the cement sheath strength and durability^{15,16}.

In this paper, the cement corrosion experiments are firstly carried out, and the corrosion depth and mechanical property evolution of the cement sample under CO₂ corrosion are measured. Secondly, a numerical model of cement sheath sealing integrity under mechanical-chemical coupling is established. The model takes into account the wellbore loading history and the dynamic evolution of cement sheath corrosion. Finally, the stress, deformation, and failure characteristics of the cement sheath under different corrosion times were analyzed. The sealing failure mechanism of cement sheath under complex loading and CO₂ corrosion is revealed. The method proposed in this paper provides valuable theoretical and technical support for the study of cement sheath integrity in CO₂ storage wells.

2. CEMENT CORROSION EXPERIMENTS

2.1 Materials and methods

Class G cement was used to make cement slurry samples in accordance with API specifications. The cement slurry was prepared according to a 0.44 water-cement ratio, and it was cured for 72 hours at 60 °C under atmospheric pressure. After curing, standard cement samples with a diameter of 25 mm and a length of 50 mm were produced by coring and grinding.

The cement sample was positioned in a high-temperature and high-pressure (HTHP) corrosion reaction kettle, and a 0.4mol/L NaCl solution was injected to simulate reservoir brine composition. Then, pass high-purity N₂ into the kettle for two hours for deoxidation treatment. The reaction kettle was subsequently heated to 90°C, and the pressure in the kettle was maintained at 15 MPa with a continuous flow of CO₂, as shown in Fig.1. The samples were taken out after 14 days and 28 days of corrosion, respectively, and the corrosion depth and mechanical parameters of the cement samples were evaluated. Note that while this section primarily presents the corrosion depth and mechanical properties of the cement samples, those interested in the microstructure, porosity, and permeability characteristics of cement after CO₂ corrosion could refer to Garnier et al., (2012), Gu et al., (2017) and Yan et al., (2023).

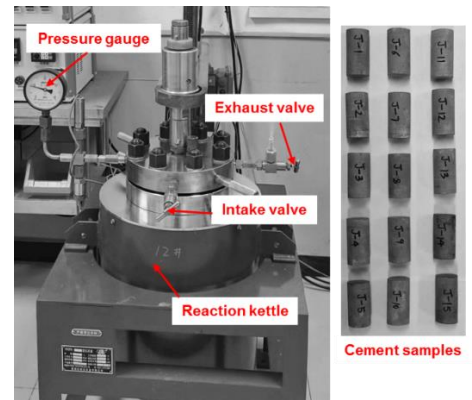


Fig. 1. HTHP corrosion curing device.

2.2 Experimental results and discussion

The SEM micrographs of the corroded cement sample were obtained by conducting SEM analysis, and the results are shown in Fig. 2. The outer zones of the cement sample become more porous and looser. This is due to the loss of calcium ions induced by supercritical CO₂ corrosion, which breaks the dense structure of the cement matrix. The inner zones of the cement sample are still relatively dense, with only a small amount of dissolved micropores. The thickness of the external corrosion layer of the sample grows with increasing corrosion time. After 14 days of corrosion, the cement corrosion depth reached 821 μm, which grew to 1.04 mm after 28 days.

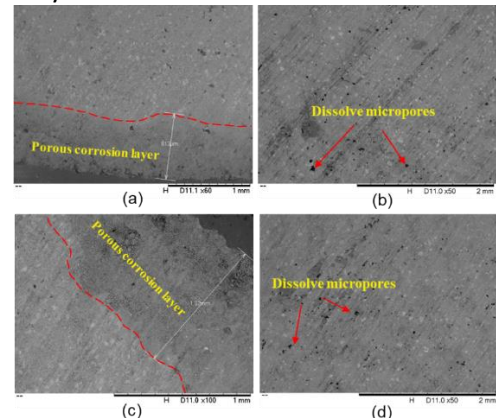


Fig. 2. SEM micrograph images of inner and outer layers.

The corrosion of the cement sheath is a long-term dynamic process during CO₂ storage. Determining the evolution of the corrosion depth of the cement sheath over a long period of time is crucial to the research of cement sheath integrity. Due to the limitation of experimental conditions and available time, the research only measured the corrosion depth of the cement sample corroded for 28 days. Barlet-Gouédard et al., (2009, 2006) conducted a corrosion test of G grade oil well cement in supercritical CO₂ using a static reactor at

90°C and 28 MPa. The results revealed that the corrosion depth varies with time is as follows:

$$L = 0.26t^{1/2}$$

where L is the corrosion depth, mm; t is the corrosion time, h.

Fig. 3 and Fig. 4 illustrates the changes in uniaxial and triaxial compressive strengths of the cement samples under various corrosion times. The results show that the uniaxial compressive strength of the cement samples was 19.208 MPa, 16.74 MPa, and 13.764 MPa when the corrosion times were 0, 14th day, and 28th day, respectively, with a -28.34% decrease in uniaxial compressive strength. Similarly, the triaxial compressive strengths of the cement specimens were 77.68 MPa, 61.75 MPa, and 40.34 MPa when the corrosion times were 0, 14th day, and 28th day, respectively, indicating a -48.06% decline in triaxial compressive strength.

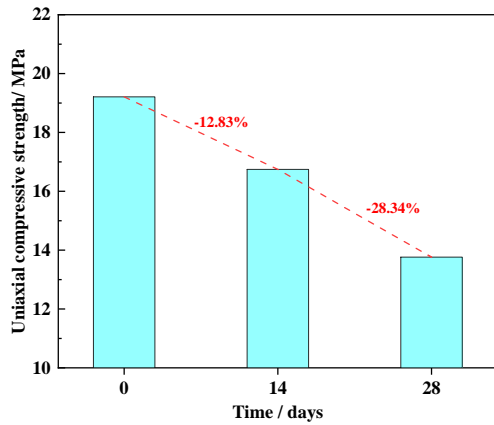


Fig. 3. Variation of uniaxial compressive strength of cement samples with time.

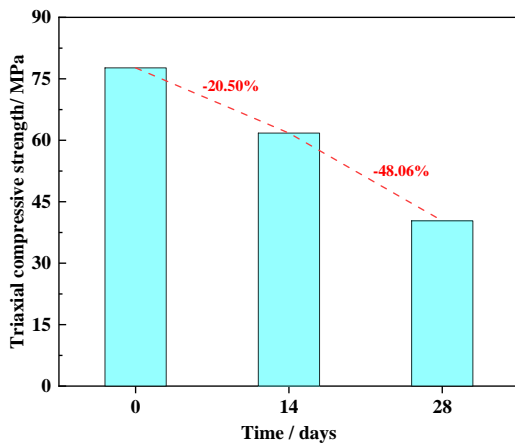


Fig. 4. Variation of triaxial compressive strength of cement samples with time.

3. MECHANICAL-CHEMICAL COUPLED CEMENT INTEGRITY MODEL

3.1 Model geometry

Assuming a symmetrical geometric model of casing-cement-formation, with no issues of casing eccentricity or cement sheath missing, and the properties of formation and cement sheath are isotropic. The established 3D casing-cement-formation numerical model is shown in Fig. 5. The inner diameter of the casing is 0.2168 m, and the outer diameter of the casing is 0.2508 m. The cement sheath has an outer diameter of 0.3112 m. To eliminate the influence of boundary effects, the length of the formation exceeds 10 times the radius of the cement sheath, and the overall model size is 2×2×0.1 m. To characterize the bonding and debonding of the cement sheath interface more accurately, the casing-cement and cement-formation interface are defined by the cohesive contact based on the traction-separation law.

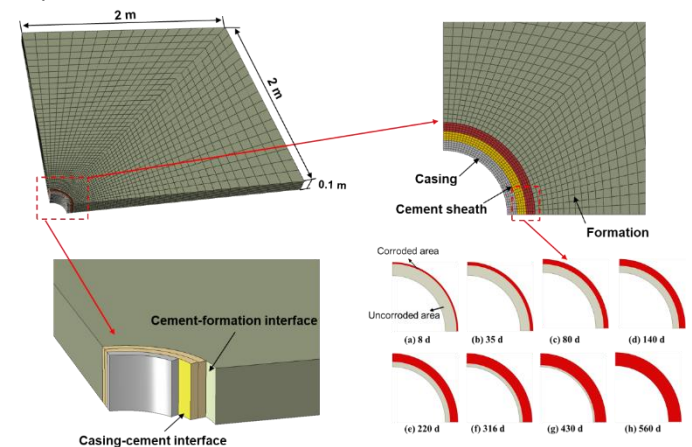


Fig. 5. Casing-cement -formation geometry model.

3.2 Material properties

The casing is an ideal elastoplastic material, the elastic properties are defined by elastic modulus and Poisson's ratio, and the yield strength is 758MPa. The formation is defined as a porosity elastoplastic material, and the plastic yielding of the rock is described using the Mohr-Coulomb criterion. The mechanical properties of the cement sheath before and after corrosion are obtained from the experiments in Section 2.2. Table 1 lists the material properties of the casing, cement before and after corrosion and formation.

Table 1 Material properties for the casing, cement, and formation

Material	Casing	Rock	Uncorroded Cement	Corroded Cement
Modulus, GPa	200	50	10.62	7.81
Poisson's	0.3	0.3	0.166	0.175
Perm, mD	–	0.1	0.001	0.1

Friction angle, degree	–	30	45.06	27.03
Cohesion, MPa	–	20	3.94	4.19

The casing-cement interface (CCI) and the cement-formation interface (CFI) are modeled using zero-thickness cohesive contacts. The properties of the cohesive interface include tensile bond strength, shear bond strength, cohesive stiffness and fracture energy, and Table 2 lists the required parameters.

Table 2 Material properties for casing/cement and cement/formation interfaces

Interface	Tensile bond strength, MPa	Shear bond strength, MPa	Cohesive stiffness, MPa	Fracture energy, J/m ²
CCI	0.50	2.00	3e5	100
CFI	0.42	0.42	3e5	100

3.3 Boundary and load conditions

Fig. 6 illustrates the wellbore whole life cycle process, including the initial state, drilling, casing, cementing, hardening/shrinkage, completion, production, and injection. The geometry and loading of the model at each stage may change, and the specific implementation process can refer to the author's previous papers^{19,20}. The corrosion of the cement sheath after CO₂ injection is a dynamic process. The corrosion depth of the cement sheath varies for different injection times, while at the same time the mechanical strength of the corroded cement is also weakened. This dynamic evolution is realized by the USDFLD subroutine.

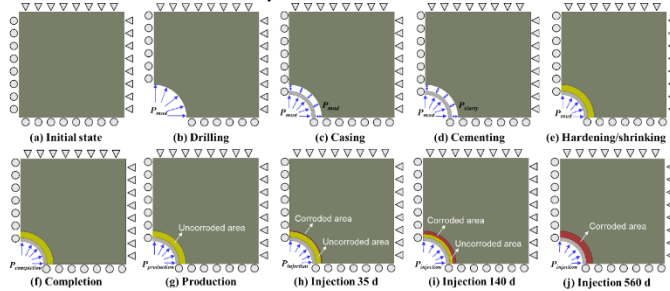


Fig. 6. Casing-cement-formation geometry model

4. RESULTS AND DISCUSSIONS

4.1 Radial stress analysis

Fig. 7 illustrates the radial stress distribution of the cement sheath under various CO₂ injection times, where the radial stress can indicate the extent of bonding and debonding at the cement sheath interface. Positive values in this study correspond to tensile stresses, and negative values represent compressive stresses. The

results show that the casing-cement interface inside the cement sheath is under compressive stress, indicating that the interface is well cemented and no micro-annulus will occur. The cement-formation interface outside the cement sheath is in tensile stress, implying that interface debonding may occur at the interface. Although the loading and boundary conditions of the model remained unchanged during the CO₂ injection, the corrosion depth of the cement sheath continued to increase, and the mechanical properties of the cement sheath decreased after corrosion. Thus, the radial stress of the cement sheath changes continuously with the injection time.

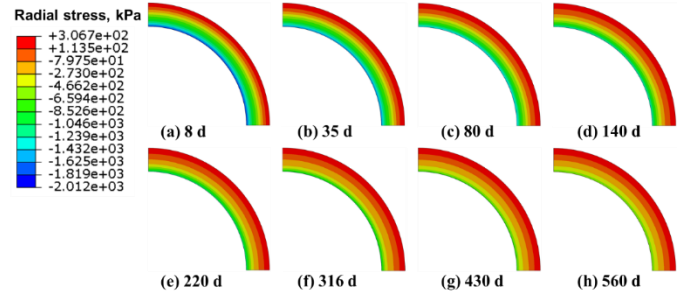


Fig. 7. Cloud maps of radial stress under different corrosion times.

Fig. 8 shows the change of radial stress along the normalized radial distance of the cement sheath at various injection times. The compressive stress at the casing-cement interface decreases gradually with the increase of injection time, and the tensile stress at the cement-formation interface increases with increasing injection time. When the injection time is 0 day, 140th day and 560th day, respectively, the compressive radial stresses inside the cement sheath are 2.01MPa, 1.31MPa and 0.62MPa, respectively. Moreover, the tensile radial stresses outside the cement sheath are 0.23MPa, 0.28MPa and 0.3 MPa, respectively. This indicates that with the increase of corrosion time, the extent of debonding at the cement-formation interface will also increase.

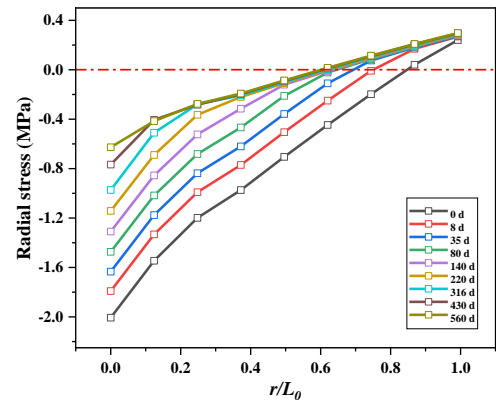


Fig. 8. The radial stress distribution of the cement along the normalized radial distance at different times.

4.2 Hoop stress analysis

Fig. 9 shows the hoop stress distribution of the cement sheath at different injection times, and the hoop stress can predict the radial tensile cracking risk of the cement sheath. The results indicate that the cement sheath is always subjected to the tensile stress in the hoop direction. The inside of the cement sheath has a higher tensile stress, with a maximum of 9.38 MPa, making it at a higher risk for radial cracking. Conversely, the outside experienced lower tensile stress, with a minimum of 3.64MPa, indicating that radial cracking is less likely to occur.

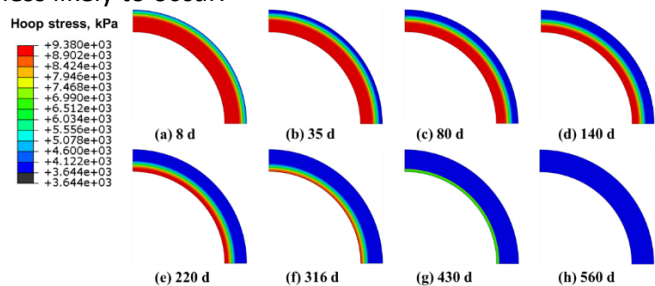


Fig. 9. Cloud maps of hoop stress under different corrosion times.

Fig. 10 illustrates the variation of hoop stress along the normalized radial distance of the cement sheath at different injection times. The results show that, except for two stages (i.e., no corrosion and complete corrosion), the hoop tensile stress gradually decreases as the normalized radial distance increases, indicating that the possibility of radial cracking of the cement sheath gradually decreases. When the CO₂ injection time was 0 day and 560th day, the hoop tensile stresses on the inside of the cement sheath were 8.89MPa and 3.64MPa, respectively, and the hoop tensile stresses on the outside of the cement sheath were 9.37MPa and 3.89MPa, respectively. The main reason is that the mechanical properties of the cement sheath are weakened after CO₂ corrosion, and the hoop stress in the corroded area is correspondingly reduced while subjected to constant external loading.

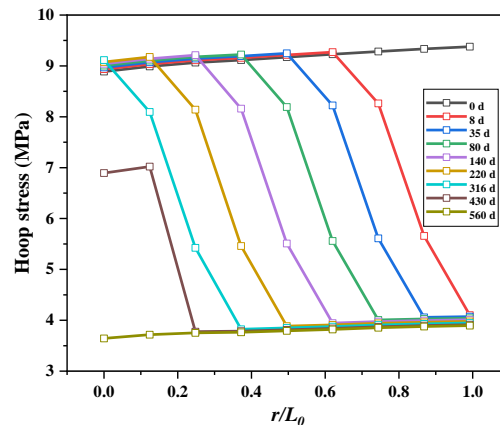


Fig. 10. The hoop stress distribution of the cement along the normalized radial distance at different times.

4.3 Interface debonding analysis

Fig. 11 shows the evolution of the micro-annulus size of the cement-formation interface along the circumference angle at different CO₂ injection times, where 0° is the direction of maximum horizontal in-situ stress, and 90° represents the direction of minimum horizontal in-situ stress. The results show that the micro-annulus size increases gradually with the increase of the circumference angle. At the start of CO₂ injection (0 days), the interfacial micro-annulus sizes at 0° and 90° directions were 91.4 μm and 103.9 μm, respectively. When CO₂ was injected for 560 days, the interfacial micro-annulus sizes at 0° and 90° directions were 102.8 μm and 115.7 μm, respectively. The interface micro-annulus size in the direction of the minimum horizontal in-situ stress is larger. This is because the in-situ stress in this direction is smaller, resulting in less pressure on the cement sheath, and the resistance to interface debonding is also smaller.

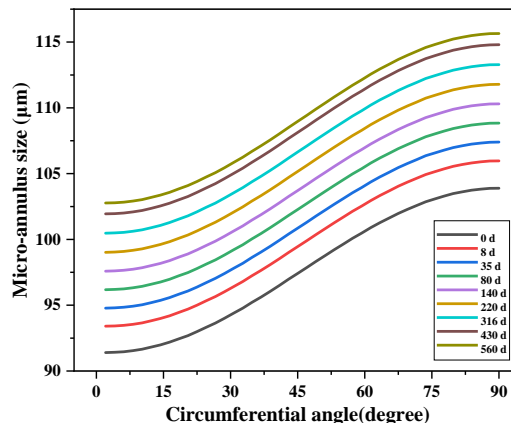


Fig. 11. The size of the micro-annulus around the well at different corrosion times

4.4 Plastic strain analysis

Fig. 12 shows the distribution of equivalent plastic strain (PEEQ) of the cement sheath at different times. PEEQ represents the accumulation of plastic strain during the entire deformation process, which can be used to indicate the plastic damage of the cement sheath. The results show that the PEEQ is smaller outside the cement sheath and larger inside the cement sheath. Meanwhile, the PEEQ is larger in the direction of the horizontal maximum in-situ stress, which is due to the higher shear stress on the inside of the cement sheath in the SH direction.

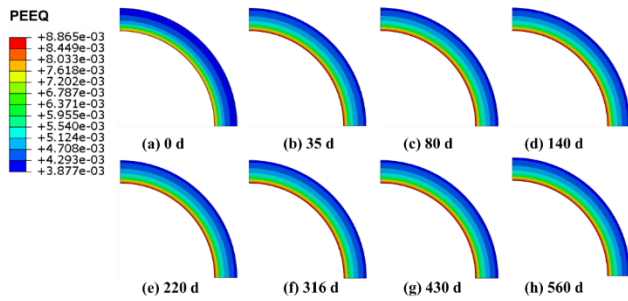


Fig. 12. Cloud maps of equivalent plastic strain under different corrosion times.

Fig. 13 shows the variation of the equivalent plastic strain of the cement sheath with corrosion time. The PEEQ of the cement sheath increases rapidly in the initial moments, followed by a gradual decline, and ultimately converges to a constant value. The observed behavior implies that the dynamic corrosion process aggravates the shear damage of the cement sheath. Nevertheless, the magnitude of PEEQ remains within a narrow range, indicating that the impact of corrosion on the shear damage is limited.

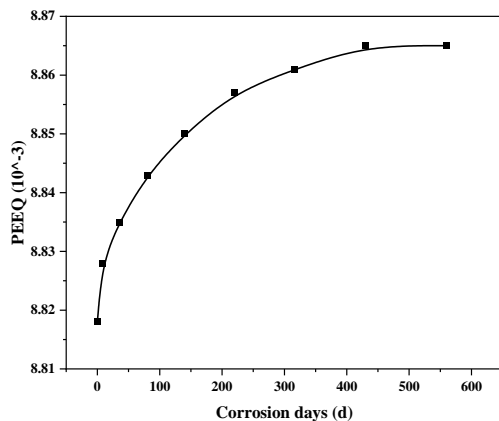


Fig. 13. The relationship between the PEEQ and corrosion time.

5. CONCLUSIONS

This paper investigates the sealing integrity of the cement sheath during the CCUS process. The cement corrosion experiments were carried out, and the

corrosion depth and mechanical parameters of the cement sheath under different corrosion times were determined. A mechanical-chemical coupled cement sheath integrity numerical model was established, and the variation of stress, deformation and damage of the cement sheath with corrosion time was discussed. The conclusions are as follows:

(1) The outer layer of the corroded cement manifests as a loosely porous feature, and the corrosion depth gradually increases with time at a gradually decreasing rate.

(2) The compressive strength, elastic modulus and friction angle of corroded cement samples gradually decreased, while Poisson's ratio and cohesion increased.

(3) The radial tensile stress, micro-annulus size and equivalent plastic strain of the cement sheath increase with corrosion time, indicating that corrosion aggravates the failure of the cement sheath.

ACKNOWLEDGEMENT

This work is supported by the National Natural Science Foundation of China (NOs. 52211530097 and 52074312).

DECLARATION OF INTEREST STATEMENT

The authors declare that they have no known competing financial interests or personal relationships that could have appeared to influence the work reported in this paper. All authors read and approved the final manuscript.

REFERENCE

- [1] Jiang K, Ashworth P, Zhang S, Liang X, Sun Y, Angus D. China's carbon capture, utilization and storage (CCUS) policy: A critical review. *Renewable and Sustainable Energy Reviews*. 2020;119:109601. doi:10.1016/j.rser.2019.109601
- [2] Nocito F, Dibenedetto A. Atmospheric CO₂ mitigation technologies: carbon capture utilization and storage. *Current Opinion in Green and Sustainable Chemistry*. 2020;21:34-43. doi:10.1016/j.cogsc.2019.10.002
- [3] Zhang Z, Pan SY, Li H, et al. Recent advances in carbon dioxide utilization. *Renewable and Sustainable Energy Reviews*. 2020;125:109799. doi:10.1016/j.rser.2020.109799
- [4] Bai M, Zhang Z, Fu X. A review on well integrity issues for CO₂ geological storage and enhanced gas recovery. *Renewable and Sustainable Energy Reviews*. 2016;59:920-926. doi:10.1016/j.rser.2016.01.043

- [5] Michael K, Golab A, Shulakova V, et al. Geological storage of CO₂ in saline aquifers—A review of the experience from existing storage operations. *International Journal of Greenhouse Gas Control*. 2010; 4(4):659-667. doi:10.1016/j.ijggc.2009.12.011
- [6] Zhang M, Bachu S. Review of integrity of existing wells in relation to CO₂ geological storage: What do we know? *International Journal of Greenhouse Gas Control*. 2011;5(4):826-840. doi:10.1016/j.ijggc.2010.11.006
- [7] Choi YS, Young D, Nešić S, Gray LGS. Wellbore integrity and corrosion of carbon steel in CO₂ geologic storage environments: A literature review. *International Journal of Greenhouse Gas Control*. 2013; 16:S70-S77. doi:10.1016/j.ijggc.2012.12.028
- [8] Li Q, Liu G. Risk Assessment of the Geological Storage of CO₂: A Review. In: Vishal V, Singh TN, eds. *Geologic Carbon Sequestration: Understanding Reservoir Behavior*. Springer International Publishing; 2016:249-284. doi:10.1007/978-3-319-27019-7_13
- [9] Alberdi-Pagola P, Fischer G. Review of Integrity Loss Detection and Quantification Due to Cracking in Cemented Wells. *SPE Journal*. Published online January 23, 2023;1-18. doi:10.2118/214303-PA
- [10] Goodwin KJ, Crook RJ. Cement Sheath Stress Failure. *SPE Drilling Engineering*. 1992;7(04):291-296. doi:10.2118/20453-PA
- [11] Yousuf N, Olayiwola O, Guo B, Liu N. A comprehensive review on the loss of wellbore integrity due to cement failure and available remedial methods. *Journal of Petroleum Science and Engineering*. 2021;207:109123. doi:10.1016/j.petrol.2021.109123
- [12] Bois AP, Garnier A, Galdiolo G, Laudet JB. Use of a Mechanistic Model To Forecast Cement-Sheath Integrity. *SPE Drilling & Completion*. 2012;27(02): 303-314. doi:10.2118/139668-PA
- [13] De Andrade J, Sangesland S. Cement Sheath Failure Mechanisms: Numerical Estimates to Design for Long-Term Well Integrity. *Journal of Petroleum Science and Engineering*. 2016;147:682-698. doi:10.1016/j.petrol.2016.08.032
- [14] Liu B, Qin J, Shi J, Jiang J, Wu X, He Z. New perspectives on utilization of CO₂ sequestration technologies in cement-based materials. *Construction and Building Materials*. 2021;272:121660. doi:10.1016/j.conbuildmat.2020.121660
- [15] Abid K, Gholami R, Choate P, Nagaratnam BH. A review on cement degradation under CO₂-rich environment of sequestration projects. *Journal of Natural Gas Science and Engineering*. 2015;27:1149-1157. doi:10.1016/j.jngse.2015.09.061
- [16] Lu B, Drissi S, Liu J, Hu X, Song B, Shi C. Effect of temperature on CO₂ curing, compressive strength and microstructure of cement paste. *Cement and Concrete Research*. 2022;157:106827. doi:10.1016/j.cemconres.2022.106827
- [17] Barlet-Gouédard V, Rimmelé G, Porcherie O, Quisel N, Desroches J. A solution against well cement degradation under CO₂ geological storage environment. *International Journal of Greenhouse Gas Control*. 2009;3(2):206-216. doi:10.1016/j.ijggc.2008.07.005
- [18] Barlet-Gouédard V, Rimmelé G, Goffé B, Porcherie O. Mitigation Strategies for the Risk of CO₂ Migration Through Wellbores. In: *OnePetro*; 2006. doi:10.2118/98924-MS
- [19] Gu C, Li X, Feng Y, Deng J, Gray K. Numerical investigation of cement interface debonding in deviated shale gas wells considering casing eccentricity and residual drilling fluid. *International Journal of Rock Mechanics and Mining Sciences*. 2022;158:105197. doi:10.1016/j.ijrmms.2022.105197
- [20] Li XR, Gu CW, Ding ZC, Feng YC. THM coupled analysis of cement sheath integrity considering well loading history. *Petroleum Science*. 2023;20(1):447-459. doi:10.1016/j.petsci.2022.09.001